

Heterostructured CoO/3D-TiO₂ nanorod arrays for photoelectrochemical water splitting hydrogen production

Jie Yan¹ · Siyuan Yang² · Zhikun Xie³ · Xin Li¹ · Wuyi Zhou¹ · Xiangchao Zhang⁴ · Yueping Fang¹ · Shengsen Zhang¹ · Feng Peng²

Received: 24 June 2016 / Accepted: 20 August 2016 / Published online: 8 September 2016
© Springer-Verlag Berlin Heidelberg 2016

Abstract Homogeneous p-type cobalt (II) oxide (CoO) nanoparticles were successfully deposited on n-type three-dimensional branched TiO₂ nanorod arrays (3D-TiO₂) through photochemical deposition and thermal decomposition to form a novel CoO/3D-TiO₂ p-n heterojunction nanocomposite. Due to the narrow band gap of CoO nanoparticles (~2.4 eV), the as-synthesized CoO/3D-TiO₂ exhibited an excellent visible light absorption. The amounts of deposited CoO nanoparticles obviously influence the hydrogen production rate in the photoelectrochemical (PEC) water splitting. The as-synthesized CoO/3D-TiO₂-5 obtains the highest PEC hydrogen production rate of 0.54 mL h⁻¹ cm⁻² after five-time CoO deposition cycles (at a potential of 0.0 V vs Ag/AgCl). The photocurrent density of CoO/3D-TiO₂-5 is 1.68 mA cm⁻¹, which is ca. 2.5 times greater than that of pure 3D-TiO₂. The results showed that the formation of internal electrical-field between the CoO/3D-TiO₂ heterojunction, which has a direction from n-type TiO₂ to p-type CoO, facilitated the charge separation and transfer and resulted in a high efficiency and stable PEC activity.

Keywords CoO nanoparticles · Three-dimensional TiO₂ nanorod arrays · p-n heterojunction · Photoelectrochemical · Water splitting

Introduction

Photoelectrochemical (PEC) water splitting hydrogen production is a promising technology to transfer solar energy to hydrogen energy. During the past decade, one-dimensional (1D) TiO₂ nanostructure (nanowire, nanorod, and nanotube) arrays have been extensively investigated to PEC water splitting hydrogen evolution due to its special advantageous properties, such as direct electrical pathways for photogenerated carriers and convenient recycling [1–4]. Furthermore, the 3D branched TiO₂ nanorod array nanostructure with increased surface area has been also attracted the attention of scientists because of its distinctive physicochemical properties [5, 6]. It is well known that pure 1D nanorod TiO₂ (rutile) arrays with the wide binding energy of 3.0 eV can hardly absorb visible light [7], which limits its efficiency of solar energy utilization. However, compared with 1D nanorod arrays, the 3D branched TiO₂ nanorod arrays with a multiple scattering effect among the branches can significantly improve the light harvesting efficiency and therefore, possess a higher photon-to-current conversion efficiency [6]. At the same time, a great deal of researches has been done to increase the visible light absorption performance of TiO₂ photocatalyst, including element-doping [8, 9], self-doping [10, 11], semiconductor-sensitizing [12, 13], and structure-varying [5, 14].

Sensitized TiO₂ nanostructure, which was modified with other narrow bandgap semiconductors, such as CdS [15, 16], Bi₂WO₆ [17], dye [18, 19], etc., displays a promising activity under visible light irradiation. Gong et al. [15] sensitize 3D TiO₂ nanorod arrays with CdS that achieve a nearly

✉ Yueping Fang
ypfang@scau.edu.cn

✉ Shengsen Zhang
zhangss@scau.edu.cn

¹ College of Materials and Energy, South China Agricultural University, Guangzhou 510642, China

² School of Chemistry and Chemical Engineering, South China University of Technology, Guangzhou 510640, China

³ Dongguang Huali Industries Co., Ltd, Dongguan 523561, China

⁴ Hunan Key Laboratory of Applied Environmental Photocatalysis, Changsha University, Changsha 410022, People's Republic of China

four times larger photocurrent than that of the pristine 3D TiO₂ nanostructure. However, the antitoxic stability of the CdS seriously influences its practical application. Recent years, due to its nontoxicity, low cost, and highly electrochemically activity, p-type semiconductor cobalt (II) oxide (CoO) with direct band gap of 2.4 eV [20, 21] received great attentions in photocatalytic field [22]. It have been demonstrated that CoO plays an important role in photocatalytic hydrogen production [21] and photodegradation of organic pollutants under visible light irradiation [22]. Ngo et al. [20] fabricated CoO/TiO₂/SrTiO₃/Si heterogeneous composite photocatalyst; the band offsets of CoO/TiO₂ was measured by in-situ XPS test and farther calculated by density functional theory (DFT). It was suggested that the deposited CoO could greatly promote the water splitting performance of TiO₂ under visible light irradiation.

In this paper, n-type 3D branched TiO₂ nanorod arrays (3D-TiO₂) modified with p-type CoO nanoparticles by a simple photochemical deposition and thermal decomposition strategy. It was indicated that benefiting from the unique p-n heterostructures and inside Schottky barriers, the as-constructed CoO/3D-TiO₂ achieved a higher photocurrent density and more excellent PEC water splitting performance than pure TiO₂ under the simulated solar light irradiation. Furthermore, to well understand the enhanced photocatalytic mechanism, a possible charge separation and transportation processes between CoO and TiO₂ were also discussed.

Experimental

Preparation of one-dimensional TiO₂ nanorod arrays

1D-TiO₂ was prepared using a modified hydrothermal method according to our previous report [1]. Ten milliliters of deionized water was mixed with 10.0 mL of concentrated hydrochloric acid (36 wt% HCl) in a Teflon-lined stainless steel autoclave (30-mL capacity) and stirred for 5 min. Then, 0.24 mL of titanium butoxide (97 % Aldrich) was introduced and stirred for another 5 min. When the solution changed to transparent, two pieces of well-cleaned FTO substrates (3.5 × 2.0 cm²) were placed against the wall of the Teflon-liner with the conductive side facing down. The sealed autoclave was kept in an oven and maintained at 170 °C for 6 h. After which, the autoclave was removed out and allowed to cool to room temperature naturally. The FTO substrates with TiO₂ nanorod was taken out and washed by deionized water.

Preparation of 3D branched TiO₂ nanorod arrays

The 3D-TiO₂ was prepared using a dip-coating method [6]. Typically, the FTO glass substrates with TiO₂ nanorod arrays were placed upside down in a beaker containing 15.0 mL of

deionized water, 15 μL of hydrochloric acid (37 wt%), and 150-μL TiCl₃ solution. The beaker was kept at 80 °C for 1 h and cooled down to room temperature naturally. Then, the sample was removed and cleaned by deionized water and ethanol to remove the surface remnant. Finally, the FTO substrates containing 3D-TiO₂ nanorod arrays were annealed in air at 350 °C for 1 h with a heating rate of 4 °C min⁻¹.

Synthesis of CoO/3D-TiO₂ heterojunction

The as-prepared 3D-TiO₂ was dipped into a 0.1-M Co(NO₃)₂ and 0.1-M ethylene glycol aqueous solution for 30 s. Then, the 3D-TiO₂ film was irradiated under UV-vis for 120 s followed by immersed in deionized water for 60 s to clean the film. The entire procedure was performed for one to several cycles to obtain a desired amount of deposition. The CoO/3D-TiO₂-X heterojunction was achieved in argon (100 sccm) atmosphere at 300 °C in a tubular furnace for 1 h with a heating rate of 5 °C min⁻¹ (X denotes the repeated deposition cycle times).

Characterization

Field-emission scanning electron microscopy (FESEM; Philips FEI Quanta 200 FEG) and transmission electron microscopy (TEM) (JEOL-2010 microscope operated at 200 kV) were used to observe the morphology and microstructure of the prepared samples. The X-ray diffraction patterns were carried out with an X-ray diffractometer (XRD; Rigaku, D/max 2500 v/pc) at a scan rate of 4 min⁻¹ in the 2θ range from 20° to 70°. The chemical nature of Co was performed with X-ray photoelectron spectroscopy (XPS) in Krato Axis Ultra DLD spectrometer with Al Kα radiation. Optical diffuse reflectance spectra were recorded by a UV-vis diffuse reflectance spectrometry (DRS; V-560, Jasco). The photoluminescence (PL) spectra were carried out using a LS 50B (Perkin Elmer, Inc., USA) with an excitation wavelength of 260 nm.

PEC performance and PEC water splitting hydrogen evolution test

In the PEC test, the CoO/3D-TiO₂-X was employed as a working electrode; a platinum wire and Ag/AgCl electrode were used as the counter electrode and reference electrode, respectively. A 0.1 M of NaNO₃ aqueous solution was used as electrolyte. A 100 mW cm⁻² of light irradiation was obtained from a simulated solar (CEL-HXF300E7, Beijing China Education Au-light Co., Ltd). An electrochemical workstation (AUTOLAB PGSTAT302) is used to measure current-voltage (I-V) characteristics of the working electrode with a scan rate of 20 mV s⁻¹. The PEC water splitting hydrogen evolution test was carried out in a CEL-SPH2N hydrogen evolution system (Beijing China Education Au-light Co., Ltd), the CoO/3D-

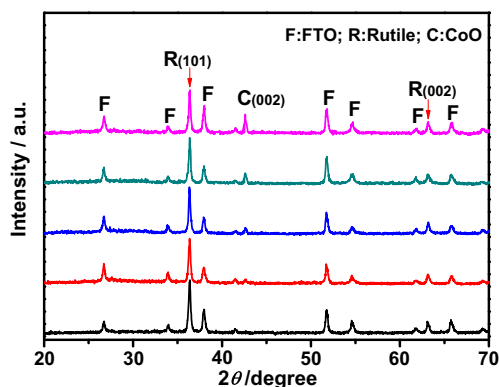


Fig. 1 XRD pattern of the as-prepared samples: 3D-TiO₂ (a), CoO/3D-TiO₂-1 (b), CoO/3D-TiO₂-3 (c), CoO/3D-TiO₂-5 (d), and CoO/3D-TiO₂-7 (e)

TiO₂-X sample flake acts as work electrode, and the gas from the Pt wire is collected by a homemade device. The device is made of a heated Pt wire and impaled in the bottom of 5-mL graduated centrifuge tube.

Results and discussion

Characterization of photocatalysts

X-ray diffraction

Figure 1 shows XRD patterns of 3D-TiO₂ nanorod arrays and CoO/3D-TiO₂-X heterojunction. The main diffraction peaks at 36.5° and 63.2° could be indexed to the (101) and (002) lattice planes of rutile TiO₂ (JCPDS No. 88-1175) after subtracting the diffraction peaks of the FTO substrate. Besides, another distinctive peak with 2θ values of 42.6° is

observed in the each CoO/3D-TiO₂-X sample, matched well with (002) lattice plane of cubic structure of CoO (JCPDS No. 48-1719). Figure 1 also displays that the intensity of the CoO characteristic diffraction peaks is enhancing as the deposition times are increasing, implying the increased loading amounts of the CoO nanocrystal.

FESEM

Figure 2 displays the FESEM images of 3D-TiO₂ and CoO/3D-TiO₂-X heterojunctions fabricated with various deposition cycles, and EDX spectrum of CoO/3D-TiO₂-5 sample. The pure 3D-TiO₂ (see in Fig. 2a) is enclosed by short needle-shaped branches with a diameter of ca. 50 nm, which improves the specific surface area of TiO₂ nanorod arrays [6]. Figure 2b–e reveals the amounts and the evolution of CoO nanoparticles deposited on 3D-TiO₂ under various photochemical deposition cycles. It clearly indicates that as the deposition cycles were increasing, the amount of CoO nanoparticles is enhancing, the needle-shaped branches are gradually covered totally by the CoO nanoparticles, and the shape changes to approximate short-rod; some of the branches even disappear completely. CoO nanoparticles congregate obviously as the deposition cycles were increasing to seven times. The EDX spectrum (see in Fig. 2e) of CoO/3D-TiO₂-5 implies that the as-prepared sample is composed of Ti, Co, and O elements (C comes from the based material of the carbon-conductive adhesives, Si and Sn come from the FTO glass substrate, and the Pt comes from Pt-sputtering of the samples before morphology observation.). No other impurity peaks are observed in both XRD and EDX patterns, revealing the fine purity of all the samples.

Fig. 2 FESEM images of the sample of 3D-TiO₂ (a), CoO/3D-TiO₂-1 (b), CoO/3D-TiO₂-3 (c), CoO/3D-TiO₂-5 (d), and CoO/3D-TiO₂-7 (e) and EDX spectrum of CoO/3D-TiO₂-5 sample (f)

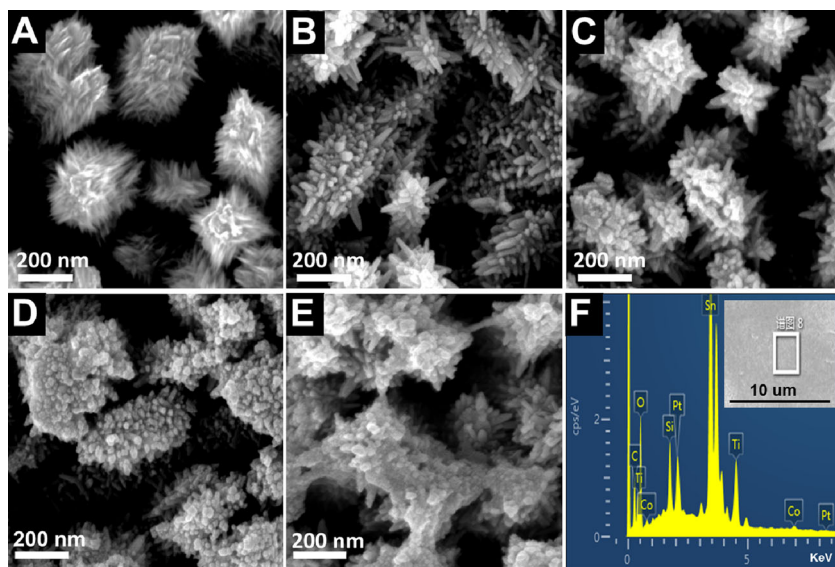
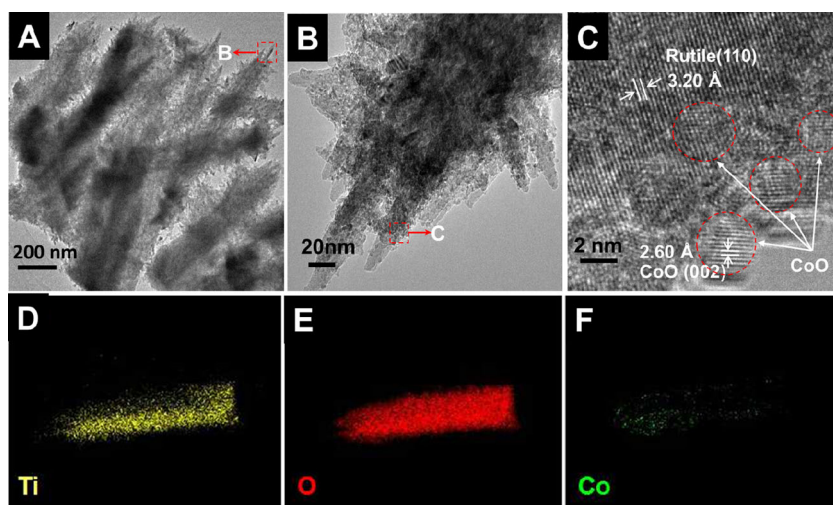


Fig. 3 TEM and HRTEM images of CoO/3D-TiO₂-5 (**a**, **b**, and **c**); the elemental mappings of Ti, O, and Co on one nanorod of CoO/3D-TiO₂-5 (**d**, **e**, and **f**)



TEM and HRTEM

As shown in Fig. 3a, the diameter of the TiO₂ trunk of 3D-TiO₂ is about 150 nm, and the length of needle-shaped branches is about 20–50 nm. Figure 3b, c shows the partially enlarged TEM images of an individual CoO/3D-TiO₂ heterojunction and corresponding HRTEM image, respectively. The size of the CoO nanoparticles is about 3.0 nm as shown in Fig. 3c. The observed lattice spacing of 3.20 Å corresponds to the (110) lattice plane of the tetragonal-rutile TiO₂ phase, and the lattice fringes of 2.60 Å correspond to the (002) lattice planes of CoO. These results further confirm that the CoO nanoparticles have been successfully loaded on the surface of 3D-TiO₂. Figure 3d–f displays the elemental mappings of Ti, O, and Co on one branched nanorod of CoO/3D-TiO₂-5 sample. It can be found clearly that Ti and O elements are uniformly distributed on the surface of the sample. The mapping of O element is the most dense among the three elements because it comes from both TiO₂ and CoO. The Co element mainly distributes at the top of the branch indicating that CoO mainly deposited on the top surface of TiO₂ branch during the photochemical deposition processing because the branches at the bottom is fewer than at the top.

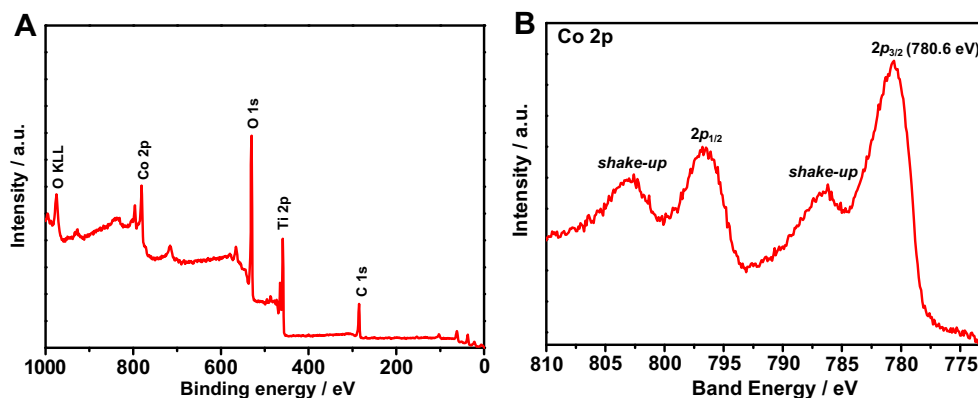
XPS

XPS analysis is performed to elucidate the chemical composition of the CoO/3D-TiO₂-5 heterojunction, and the spectra are presented in Fig. 4. All of the O, Co, and Ti elements are observed in Fig. 4a, and the presence of C element can be mainly ascribed to the adventitious hydrocarbon from XPS itself. Figure 4b shows the high-resolution XPS spectra of Co 2p. It is implied that the binding energies of the main peaks are located at 780.6 and 796.8 eV corresponding to Co 2p_{3/2} and Co 2p_{1/2} levels, respectively, and the peaks located at 786.6 and 803.2 eV are marked as the Co 2p_{3/2} and Co 2p_{1/2} satellite peaks, respectively [20, 23]. The 2p binding energy position in conjunction with the very strong satellite at 6 eV is consistent with Co being in the +2 valence state with high spin [20, 23]. These results indicate that the heterojunction is consisted of TiO₂ and CoO.

UV-Vis diffuse reflectance spectra

The UV-vis diffuse reflectance spectra (UV-vis DRS) of 3D-TiO₂ and CoO/3D-TiO₂-X samples are illustrated in Fig. 5. The 3D-TiO₂ sample shows the typical absorption

Fig. 4 Whole XPS spectrum (a) and Co 2p XPS spectrum (b) of CoO/3D-TiO₂-5



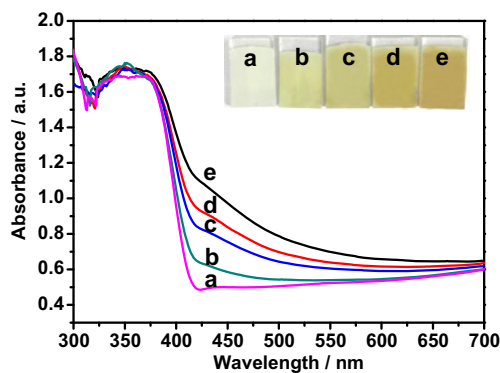


Fig. 5 UV-vis absorption spectra of different samples and corresponding optical photographs (insets): 3D-TiO₂ (a), CoO/3D-TiO₂-1 (b), CoO/3D-TiO₂-3 (c), CoO/3D-TiO₂-5 (d), and CoO/3D-TiO₂-7 (e)

of rutile in the UV region due to the transition of the electron from the valence band to the conduction band. After CoO nanoparticles are deposited onto the 3D-TiO₂, the light absorption ability of the sample is enhanced greatly in visible light region. The absorption intensity of as-synthesized CoO/3D-TiO₂-X samples in visible region is strengthened as the CoO photochemical deposition cycles were increasing, which is mainly resulted by the light yellow color of CoO (see the insets of Fig. 5), indicating that the deposition of CoO can strongly affect the visible light absorption of the 3D-TiO₂, but exhibits almost no impact on UV light absorption.

Photoluminescence spectrum

Photoluminescence (PL) spectrum is an effective method usually applied to investigate the lifetime of charge carriers and separation efficiency of the photogenerated electron/hole pairs of the photocatalysts [24]. Figure 6 displays the PL emission spectra of as-prepared 3D-TiO₂ and CoO/3D-TiO₂-5 samples at an excitation wavelength

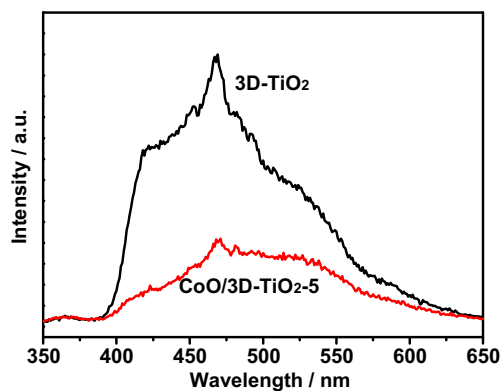


Fig. 6 Photoluminescence spectra of the 3D-TiO₂ and CoO/3D-TiO₂-5 samples

of 260 nm. It can be seen that the PL emission intensities of CoO/3D-TiO₂-5 are much weaker than that of 3D-TiO₂, indicating that the CoO/3D-TiO₂-5 possesses lower recombination rate of photoinduced electrons and holes than that of 3D-TiO₂.

Photoelectrochemical activity

Figure 7a displays a set of linear sweep voltammograms (LSV) for 3D-TiO₂ and CoO/3D-TiO₂-X samples. It presents the influence of the deposition amounts of CoO nanoparticles on PEC performance of 3D-TiO₂. In the control experiments,

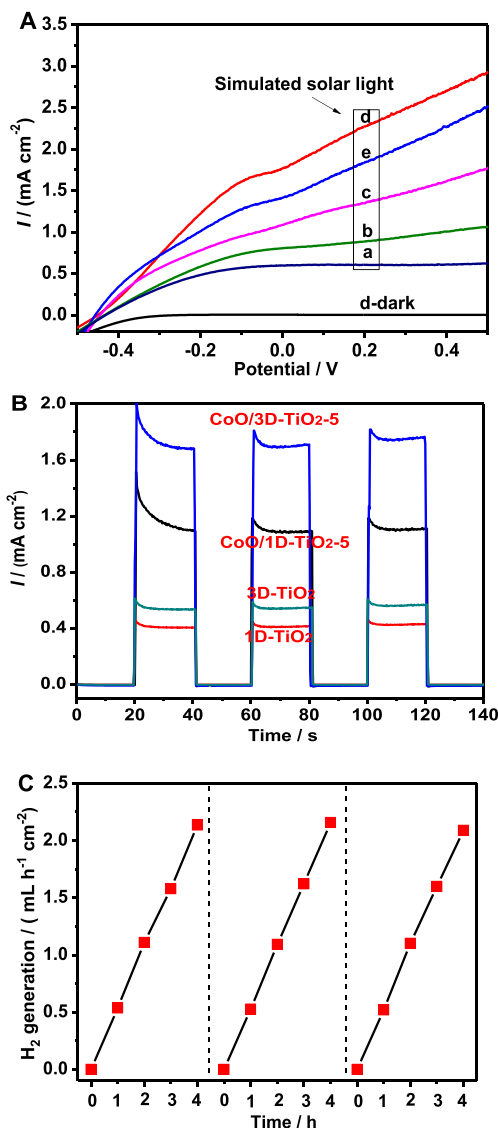


Fig. 7 a Linear sweep voltammograms at a scan rate on different samples 3D-TiO₂ (a), CoO/3D-TiO₂-1 (b), CoO/3D-TiO₂-3 (c), CoO/3D-TiO₂-5 (d), and CoO/3D-TiO₂-7 (e). b Photocurrent density profiles of 1D-TiO₂, 3D-TiO₂, CoO/1D-TiO₂-5, and CoO/3D-TiO₂-5 samples. c Measured H₂ production and the reusability of the CoO/3D-TiO₂-5 at 0.0 V vs Ag/AgCl under the light of 100 mw cm⁻² irradiation

the dark current from -0.5 to 0.5 V of each sample is almost zero. For the pure 3D-TiO₂ sample, the photocurrent (I) intensity is 0.53 mA cm^{-1} at a potential of 0.0 V vs. Ag/AgCl under the simulated solar light irradiation (see in Fig. 7a (a)). After CoO nanoparticles were being deposited, the PEC activity of the 3D-TiO₂ increases remarkably, and the photocurrent increases gradually as the deposition cycles were increasing from 1 to 5 under light irradiation, and then declines evidently when the deposition cycles further increase to 7. At a potential of 0.0 V, the maximum PEC activity of CoO/3D-TiO₂-5 is 1.68 mA cm^{-1} , which is ca. 2.5 times larger than that of 3D-TiO₂ as shown in Fig. 7a (d). Though the absorption intensity of CoO/3D-TiO₂-7 is stronger than that of CoO/3D-TiO₂-5 (see Fig. 5), the CoO/3D-TiO₂-7 possesses lower photoelectrocatalytic efficiency than that of the CoO/3D-TiO₂-5. It can be explained by the remarkable congregation of the CoO nanoparticles on the surface of CoO/3D-TiO₂-7 compared to that on the surface of CoO/3D-TiO₂-5, as shown in Fig. 2d, e. The obvious congregation results in the reduction of the specific surface area and the increase of the transmission distance of the photogenerated electrons, which will influence the photocatalytic performance of the sample dramatically. The former will decrease the number of surface active sites of CoO/3D-TiO₂ photocatalyst; the latter will weaken the intensity of internal electric field in p-n heterojunction and enhance photogenerated electron-hole pair recombination in both TiO₂ and CoO.

The photoelectrochemical properties of TiO₂ nanorod arrays (1D-TiO₂) could be affected by the lengths and diameters of the nanorod, and the surface areas and the degree of aggregation at the base of the TiO₂ nanorods [25, 26]. Compared with 1D-TiO₂, 3D-TiO₂, which was based on 1D-TiO₂, possesses higher surface area and enhanced photocurrent harvest efficiencies [15, 27]. In order to investigate the role of the branches of the 3D-TiO₂, the photocurrent of 1D-TiO₂, 3D-TiO₂, CoO/1D-TiO₂-5, and CoO/3D-TiO₂-5 was measured. Figure 7b shows that there is no current in darkness for the four samples.

While under the light irradiation and a bias potential of 0.0 (vs. Ag/AgCl), an exceptionally high photocurrent response was observed. Moreover, the photocurrent of both 1D-TiO₂ and CoO/1D-TiO₂-5 is lower than that of 3D-TiO₂ and CoO/3D-TiO₂-5, respectively. The branches in 3D-TiO₂ can significantly improve photon-to-current conversion efficiency, even its nanocomposites.

The photoelectrochemical water splitting hydrogen production rate and its stability as CoO/3D-TiO₂-5 sample employed as work electrode are investigated. Under the light irradiation, gas bubbles can be observed at the Pt wire electrode. The gas emitted from the Pt wire is collected by a homemade device. Figure 7c indicates that the CoO/3D-TiO₂-5 exhibits a high PEC hydrogen production rate of $0.54 \text{ mL h}^{-1} \text{ cm}^{-2}$ at the first run. And the hydrogen production rate is well maintained after three runs, suggesting that the CoO/3D-TiO₂-5 heterojunction possesses good stability and reusability. This indicates that the 3D-TiO₂ loaded with CoO nanoparticles possesses higher PEC performance toward water splitting hydrogen production under the simulated solar light irradiation.

Mechanism of formation of CoO and PEC hydrogen production

Mechanism of formation of CoO

The characterization of XRD, HRTEM, and XPS confirms that the nanoparticles on 3D-TiO₂ are CoO nanoparticles. To understand the formation process of CoO by the photochemical deposition and thermal decomposition in argon atmosphere method, the detailed reaction steps are proposed as follows:

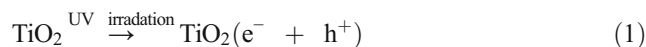
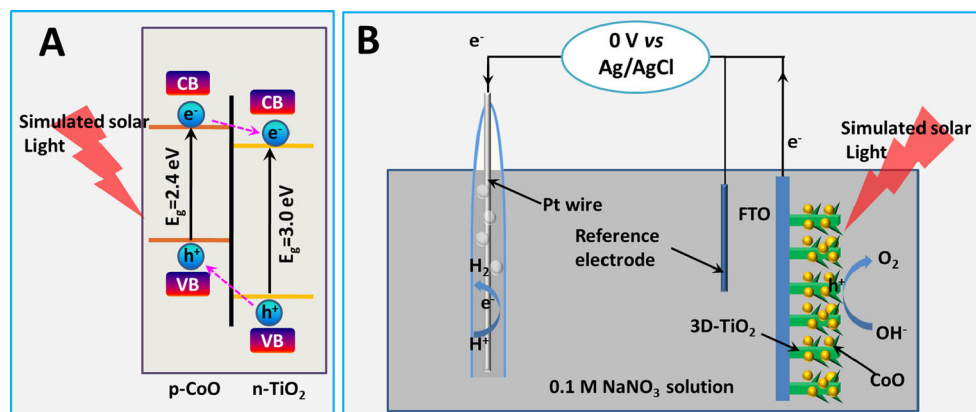


Fig. 8 Scheme of the interaction between CoO and TiO₂ (a) and high PEC water splitting system of CoO/3D-TiO₂ (b)





Under UV light irradiation, photogenerated electrons (e^-) in the VB of TiO_2 are excited to the CB, leaving only holes (h^+) in the VB. The e^- reduction H_2O to H_2 and OH^- and the h^+ are primarily scavenged by ethylene glycol (as electron donors) in the reaction solution. The OH^- contacts with the Co^{2+} from $\text{Co}(\text{NO}_3)_2$ and forms an insoluble $\text{Co}(\text{OH})_2$ on the surface of 3D- TiO_2 , and then the thermal decomposition of $\text{Co}(\text{OH})_2$ produces H_2O and CoO in argon atmosphere [28].

Mechanism of PEC hydrogen production

The interaction between CoO and TiO_2 and high PEC water splitting performance of $\text{CoO}/3\text{D-TiO}_2$ has been discussed as follows. As shown in Fig. 8a CoO is an important p-type semiconductor ($E_g = 2.4$ eV), and rutile TiO_2 is a typical n-type semiconductor ($E_g = 3.0$ eV); they can be excited under visible light and UV light irradiation, respectively. After TiO_2 loaded with CoO nanoparticles, a p-n heterojunction between the two semiconductors is formed, and an internal electric field with direction from TiO_2 to CoO exists in p-n junction. In addition, the CB and VB of CoO are both higher than that of TiO_2 respectively. These two factors promote the photogenerated electron on CB of CoO transferring to that of TiO_2 and photogenerated holes on VB of TiO_2 transferring to that of CoO under the simulated solar light irradiation, and decrease the recombination of photogenerated electron–hole pairs. In the PEC system (Fig. 8b), the separated photogenerated electrons transfer from $\text{CoO}/3\text{D-TiO}_2$ to the Pt wire via external circuit at 0.0 V bias, and then transform the H^+ to H_2 . The separated holes on VB of CoO will oxidize OH^- as a result of evolution of oxygen.

Conclusions

Homogeneous p-type CoO nanoparticles were successfully deposited on n-type three-dimensional branched TiO_2 nanorod arrays through photochemical deposition and thermal decomposition methods. The novel $\text{CoO}/3\text{D-TiO}_2$ p-n heterojunction nanocomposite exhibited an excellent light absorption. Under the simulated solar light of 100 mW cm^{-2} , the photocurrent density of the $\text{CoO}/3\text{D-TiO}_2$ -5 photoanode increases from 0.53 to 1.68 mA cm^{-1} , and the PEC hydrogen production rate of $0.54 \text{ mL h}^{-1} \text{ cm}^{-2}$ is obtained. These results can be attributed to the reduced recombination of photogenerated electrons and holes owing to the p-n heterojunction of $\text{Co}/3\text{D-TiO}_2$. This work will also offer an attractive perspective for applications of the p-n heterojunction nanocomposite in solar cells or photocatalysts.

Acknowledgments This work was supported by the financial support from the NSFC (No. 21328301), the Guangdong Provincial Science and Technology Project (Nos. 2016A010104013 and 2015A050502012), the Foundation of Guangdong Traffic Science and Technology (No. 2015-02-016), and the Open Research Fund of Hunan Key Laboratory of Applied Environmental Photocatalysis (CCSU-XT-06), Changsha University.

References

1. Wang G, Xiao X, Li W, Lin Z, Zhao Z, Chen C, Wang C, Li Y, Huang X, Miao L, Jiang C, Huang Y, Duan X (2015) *Nano Lett* 15:4692–4698
2. Mali SS, Shim CS, Park HK, Heo J, Patil PS, Hong CK (2015) *Chem Mater* 27:1541–1551
3. Zheng Q, Zhou B, Bai J, Li L, Jin Z, Zhang J, Li J, Liu Y, Cai W, Zhu X (2008) *Adv Mater* 20:1044–1049
4. Balogun MS, Zhu Y, Qiu W, Luo Y, Huang Y, Liang C, Lu X, Tong Y (2015) *ACS Appl Mater Inter* 7:25991–26003
5. Pan X, Xu YJ (2015) *J Phys Chem C* 119:7184–7194
6. Cho IS, Chen Z, Forman AJ, Kim DR, Rao PM, Jaramillo TF, Zheng X (2011) *Nano Lett* 11:4978–4984
7. Liu H, Lian G (2004) *J Am Ceram Soc* 87:1582–1584
8. Deng L, Wang S, Liu D, Zhu B, Huang W, Wu S, Zhang S (2009) *Catal Lett* 129:513–518
9. Szirmai P, Horváth E, Náfrádi B, Micković Z, Smajda R, Djokić DM, Schenk K, Forró L, Magrez A (2013) *J Phys Chem C* 117:697–702
10. Liu N, Schneider C, Freitag D, Hartmann M, Venkatesan U, Muller J, Spiecker E, Schmuki P (2014) *Nano Lett* 14:3309–3313
11. Gurylev V, Su CY, Perng TP (2015) *J Catal* 330:177–186
12. Qamar M, Dmrosh Q, Ahmed MI, Qamaruddin M, Yamani ZH (2015) *Nanoscale Res Lett* 10:1–6
13. Liu S, Zhu J, Guo X, Ge J, Wu H (2015) *Colloid Surface A* 484:434–440
14. Tu W, Zhou Y, Liu Q, Yan S, Bao S, Wang X, Xiao M, Zou Z (2013) *Adv Funct Mater* 23:1743–1749
15. Su F, Lu J, Tian Y, Ma X, Gong J (2013) *Phys Chem Chem Phys* 15:12026–12032
16. Qian X, Qin D, Bai Y, Li T, Tang X, Wang E, Dong S (2001) *J Solid State Electrochem* 5:562–567
17. Shang M, Wang W, Zhang L, Sun S, Wang L, Zhou L (2009) *J Phys Chem C* 113:14727–14731
18. Wang H, Bai Y, Wu Q, Zhou W, Zhang H, Li J, Guo L (2011) *Phys Chem Chem Phys* 13:7008–7013
19. Lan Z, Wu W, Zhang S, Que L, Wu J (2016) *J Solid State Electrochem*. doi:10.1007/s10008-016-3263-y
20. Ngo TQ, Posadas A, Seo H, Hoang S, Medaniel MD, Utess D, DH Triyoso, C Buddie Mullins, AA Demkov, JG Ekerdt (2013) *J Appl Phys* 114:084901–084908
21. Liao L, Zhang Q, Su Z, Zhao Z, Wang Y, Li Y, Lu X, Wei D, Feng G, Yu Q, Cai X, Zhao J, Ren Z, Fang H, Robles-Hernandez F, Baldelli S, Bao J (2014) *Nat Nanotechnol* 9:69–73
22. Zhou C, Zhang Y, Li Y, Liu J (2013) *Nano Lett* 13:2078–2085
23. Barreca D, Massignan C, Daolio S, Fabrizio M, Piccirillo C, Armelao L, Tondello E (2001) *Chem Mater* 13:588–593
24. Zhang S, Peng B, Yang S, Fang Y, Peng F (2013) *Int J Hydrogen Energ* 38:13866–13871
25. Wang X, Zhang S, Wang H, Yu H, Wang H, Zhang S, Peng F (2015) *RSC Adv* 5:76315–76320
26. Hoang S, Guo SW, Hahn NT, Bard AJ, Mullins CB (2012) *Nano Lett* 12:26–32
27. Hwang YJ, Hahn C, Liu B, Yang P (2012) *ACS Nano* 6:5060–5069
28. Zhang G, Huang H, Li W, Yu F, Wu H, Zhou L (2012) *Electrochim Acta* 81:117–122